Impact of brain tissue filtering on neurostimulation fields: A modeling study

Citation: Wagner, Tim, Uri Eden, Jarrett Rushmore, Christopher J. Russo, Laura Dipietro, Felipe Fregni, Stephen Simon, et al. "Impact of Brain Tissue Filtering on Neurostimulation Fields: A Modeling Study." NeuroImage 85 (January 2014): 1048–1057.

As Published: http://dx.doi.org/10.1016/j.neuroimage.2013.06.079

Publisher: Elsevier

Persistent URL: http://hdl.handle.net/1721.1/99416

Version: Author's final manuscript: final author's manuscript post peer review, without publisher's formatting or copy editing

Published in final edited form as:
Neuroimage. 2014 January 15; 85(0 3): 1048–1057. doi:10.1016/j.neuroimage.2013.06.079.

Impact of brain tissue filtering on neurostimulation fields: a modeling study

Tim Wagner[1,2,*], **Uri Eden**[3], **Jarrett Rushmore**[4], **Christopher J. Russo**[2], **Laura Dipietro**[5], **Felipe Fregni**[6], **Stephen Simon**[1,4], **Stephen Rotman**[6], **Naomi B. Pitskel**[6], **Ciro Ramos-Estebanez**[6], **Alvaro Pascual-Leone**[6,9], **Alan J. Grodzinsky**[7,8], **Markus Zahn**[7], and **Antoni Valero-Cabre**[4]

[1]Highland Instruments, Cambridge, MA

[2]Division of Health Sciences and Technology, Harvard Medical School/Massachusetts Institute of Technology, Boston, MA

[3]Department of Mathematics and Statistics, Boston University, Boston, MA

[4]Lab. Cerebral Dynamics, Plasticity and Rehabilitation, Boston University School of Medicine, Boston, MA

[5]Department of Mechanical Engineering, Massachusetts Institute of Technology, Cambridge, MA

[6]Harvard Medical School, Boston, MA

[7]Department of Electrical Engineering and Computer Science, Massachusetts Institute of Technology, Cambridge, MA

[8]Center for Biomedical Engineering, Massachusetts Institute of Technology, Cambridge, MA

[9]Berenson-Allen Center for Noninvasive Brain Stimulation, Beth Israel Deaconess Med Ctr, Boston, MA

Abstract

Electrical neurostimulation techniques, such as deep brain stimulation (DBS) and transcranial magnetic stimulation (TMS), are increasingly used in the neurosciences, e.g., for studying brain function, and for neurotherapeutics, e.g., for treating depression, epilepsy, and Parkinson's disease. The characterization of electrical properties of brain tissue has guided our fundamental understanding and application of these methods, from electrophysiologic theory to clinical dosing-metrics. Nonetheless, prior computational models have primarily relied on ex-vivo impedance measurements. We recorded the *in-vivo* impedances of brain tissues during neurosurgical

[*]Corresponding Authorship: Tim Wagner, twagner@mit.edu PO Box 381933 Cambridge, MA 02238 (t)617-504-6031.

Commercial Interest: In addition to Dr. Timothy Wagner's positions at Harvard Medical School and MIT, he is the Chief Science Officer of Highland Instruments, a medical device company. He has multiple patents and/or patents pending related to imaging, brain stimulation, and wound healing.

procedures and used these results to construct MRI guided computational models of TMS and DBS neurostimulatory fields and conductance-based models of neurons exposed to stimulation. We demonstrated that tissues carry neurostimulation currents through frequency dependent resistive and capacitive properties not typically accounted for by past neurostimulation modeling work. We show that these fundamental brain tissue properties can have significant effects on the neurostimulatory-fields (capacitive and resistive current composition and spatial/temporal dynamics) and neural responses (stimulation threshold, ionic currents, and membrane dynamics). These findings highlight the importance of tissue impedance properties on neurostimulation and impact our understanding of the biological mechanisms and technological potential of neurostimulatory methods.

Keywords

Neuromodulation; Neurostimulation; TMS; DBS; Cellular models

1. Introduction

Exogenous brain stimulation techniques, such as deep brain stimulation (DBS) and transcranial magnetic stimulation (TMS), have been successfully used to study essential properties of the nervous system and to treat numerous neurological disorders, such as Parkinson's disease with DBS and depression with TMS (Kuncel and Grill, 2004; Wagner et al., 2007). Underlying all of these techniques is the necessity to understand how stimulatory electromagnetic fields interact and pass through tissue(s) to effectively influence targeted neural circuits at a distance from the stimulation source (Butson and McIntyre, 2005; Tehovnik, 1996; Wagner et al., 2007).

In biological tissues, electric fields drive currents with ohmic (resistive) and displacement (capacitive) components. Ohmic currents are generated by the movement of free charges, such as unbound extracellular sodium and potassium ions. Electrical conductivity is a measure of how easily these free charges move through the medium. Displacement currents are generated by the polarization of paired charges, such as ionic double-layers that surround cellular membranes and/or macromolecules embedded in cellular membranes (for a further discussion of mechanisms see (Foster and Schwan, 1989, 1996; Pethig and Kell, 1987; Schwan, 1963)). Electrical permittivity is a measure related to how easily these paired charges are polarized. Most biophysical theories of brain stimulation, from those guiding our understanding of essential biological mechanisms to those guiding clinical safety and dosing criteria, assume that stimulating currents are entirely ohmic and consider displacement currents to have essentially no role in the stimulation of neural tissue. This assumption is largely based on ex-vivo tissue impedance measurements, in which measured permittivities predict displacement currents to be orders of magnitude smaller than their ohmic counterparts in the spectral frequency band of the applied stimulatory fields (Heller and Hulsteyn, 1992; Plonsey and Heppner, 1967; Wagner et al., 2007; Wagner et al., 2004).

However, experimental work and theoretical studies from the material sciences suggest that within the electromagnetic field frequency band used for brain stimulation, the displacement currents may in fact be significant enough to impact the stimulatory fields ((IFAP), 2007;

Butson and McIntyre, 2005; Foster and Schwan, 1989, 1996; Pethig and Kell, 1987; Wagner et al., 2004) -please note that IFAP stands for the Institute for Applied Physics (http://niremf.ifac.cnr.it/tissprop/). Schwan was the first to demonstrate this elevated tissue permittivity with decreased frequency, thought to result from relaxation of counterions tangential to the cell membranes in tissues (*i.e.*, alpha dispersion) (Foster and Schwan, 1989, 1996; Pethig and Kell, 1987; Schwan, 1954, 1963). Furthermore, *in-vivo* recordings of the electromagnetic fields generated in brain tissues by TMS (Tay, 1992; Tay, 1989) and DBS (Miocinovic et al., 2009) both suggest the stimulatory fields are influenced by both tissue capacitance and resistance. This indicates that past theories of brain stimulation may not fully account for fundamental biophysical processes occurring in neural tissue; which, could impact the predicted network response and the safety/dosing profiles that guide the clinical use of brain stimulation (Wagner et al., 2007). Furthermore, coupled displacement and ohmic mechanisms in neural tissue could lead to frequency dependent filtering of the applied stimulatory fields, or endogenously generated fields (Bedard et al., 2004; Bossetti et al., 2008; De Geeter et al., 2012; Foster and Schwan, 1996; Grant and Lowery, 2010; Tracey and Williams, 2011; Wagner et al., 2004). Such filtering effects could alter a predicted stimulatory waveform's size and shape, impacting the expected neural response and electrochemical interactions taking place in the brain. In this study, we recorded in-vivo head and brain tissue impedance properties throughout the neurostimulation frequency range and assessed their impact on the mechanisms of neural stimulation and metrics guiding its use.

2. Materials and Methods

We first measured the conductivity,σ, and permittivity, ε, values of tissues, in the frequency range from 10 to 50,000 Hz, in anesthetized animals. We then constructed MRI guided finite element models (FEMs) of the electromagnetic fields generated during TMS and DBS based on the individual tissue impedance properties we recorded and, for comparison, with impedance values used in past modeling studies, primarily developed from ex-vivo measurements. We then evaluated how these tissue properties affect the TMS and DBS stimulatory fields. Finally, we explored the effects of the tissues and resulting field responses on stimulation thresholds and response dynamics of a conductance based model of the human motor neuron (see Supplementary Methods, Supplementary Figure 1 (i.e., Sup. Fig.1)).

2.1 Tissue Recordings

Two adult cats were obtained from licensed cat breeders (Liberty Laboratories, Waverly, NY). Neurosurgical/craniotomy procedures, detailed in (Rushmore et al., 2006), and approved by the Boston University School of Medicine IACUC committee, were conducted. Anaesthetized (4% isoflurane in 30% oxygen and 70% nitrous oxide) animals' head/brain tissues were exposed and a specialized impedance probe, fabricated from a modified forceps, was applied.

At low electromagnetic field frequencies, typical of brain stimulation sources, the characterization of tissue impedances is complicated by the potential for large electrode polarization artifacts, even in four-terminal measurements (see, e.g., (Pethig and Kell, 1987;

Schwan, 1963)), which can be further complicated by nonlinear electrode materials (Schwan, 1966, 1968), needle microelectrode effects (Schwan, 1966, 1968), and measurement electronics (Pethig and Kell, 1987; Schwan, 1963; Schwan and Ferris, 1968). For our measurements, we followed the method detailed in (Gabriel et al., 1996b) to account for polarization artifacts in the probe. We also used a material well characterized in our recording band for our impedance probe interface (i.e., platinum) (Schwan, 1966, 1968, 1992), used modified forceps without the pronounced geometrical constraints of needle microelectrodes (Schwan, 1966, 1968), and implemented a recording system (Hewlett Packard HP4192A) capable of resolving impedance in the spectrum analyzed, all detailed below.

First, the tissue impedance probe was produced by modifying a self-closing forceps mechanism (Dumont N5) for use as a controllable, two plate sputtered platinum probe to limit polarization effects (Schwan, 1992). Probe tips were created by cutting the tips off of the stainless steel forceps and coating the inside faces using electron beam evaporation. The tips were coated under high vacuum conditions (5 ×10-7 torr) with 10nm Titanium (99.99% Alfa Aesar) as an adhesion layer and then 50nm of Platinum (99.99% Alfa Aesar). The tips were then re-attached to the closing mechanism using two plastic adapter plates, providing electrical insulation from proximal instruments and tissues. The self-closing handle mechanism was also modified using two fine-threaded screws to allow for precise and repeatable control of the inter-electrode separation distance. Further control was achieved by fixing the impedance probe to a micropositioner (Kopf, Tujunga, CA). Overall, soft tissue sample volume was maintained constant at 50 μm × 200 μm × 400 μm (+/- 10 μm on the larger dimensions). Prior to the animal recordings, the probe's transfer function was characterized from 0.01 to 50kHz in saline solutions from 0.0 (deionized) to 0.09 molar NaCl, to account for electrode polarization effects (Schwan, 1992), via the substitution/ subtraction technique methods directly outlined in (Gabriel et al., 1996b).

The probe was used as a surgical instrument to systematically grasp and isolate the tissues, where they were investigated with an HP4192A impedance analyzer (Hewlett Packard, Palo Alto) to determine the tissue impedances (conductivity and permittivity) of the skin, skull, gray matter, and white matter following methods similar to (Gabriel et al., 1996b). Tissue measurements were primarily taken along the radial axis for the skin and bone and approximately tangential to the tissue boundary for gray matter and white matter. Tissue anisotropy was not explored in this current study, to minimize proximal tissue disturbance with our probe, and was left for future studies. Recordings were taken from 10 to 50,000 Hz to span the typical brain stimulation power spectrum, at 75 logarithmically spaced points on the frequency log scale (20 points per decade). Approximately 8 separate sweeps per cat and tissue were performed across the frequency band. Average values of the conductivity and permittivity were then calculated for each frequency. Saline measurements were repeated throughout the experiment, and the probe was examined for integrity under a surgical microscope between measurements (approximately every 8 recordings). For each tissue, an additional 3-4 sweeps were made at 5 Hz steps (30,000-40,000 additional points), throughout the procedures, to validate the trends presented herein. During the procedures, the effects of in-vivo tissue injury/death were also explored (Sup.Fig.2).

2.2 Transient Electromagnetic Field Solutions

We constructed MRI guided FEMs of the human head based on the individual tissue impedance properties recorded in-vivo and with ex-vivo impedance values to determine the electromagnetic fields generated during TMS and DBS (the ex-vivo values span the range of those which have served as the basis of neurostimulation theory (Wagner et al., 2007; Wagner et al., 2004)). Fifteen different waveforms commonly used during DBS and TMS stimulation were explored as current constrained TMS coil inputs (3 kA peak), and voltage (0.2 V p-p maximum) and current (0.1 mA p-p maximum) constrained DBS electrode inputs (i.e., we explored the same input waveform shape for the TMS and DBS conditions), Fig. 1. Although DBS stimulators normally operate as voltage constrained devices, we analyzed both current and voltage constrained systems (i.e., current constrained refers to the current at the DBS electrode contacts being controlled such that only the voltage can vary due to the boundary/tissue effects, and voltage constrained refers to the voltage being fixed such that only the current can vary due to the boundary/tissue effects). First, the time domain input waveforms were converted to the frequency domain via discrete Fourier transforms in the Mathworks MATLAB computing environment. Second, the field responses of the individual frequency components to different tissue impedance sets were analyzed in the sinusoidal steady state in 10 Hz increments, between 0-50kHz, with separate TMS and DBS sinusoidal steady state (SSS) FEMs based on MRI guided CAD renderings of the human head explored with a MATLAB controlled Ansoft 3D Field Simulator. Each individual frequency component solution was determined via a Matlab controlled Ansoft field solvers (TMS via a modified magnetic diffusion equation implementing a modified T-Ω method, and the DBS solutions via a modified Laplacian, see (Wagner et al., 2007; Wagner et al., 2004) and/or the supplementary methods section. Examples of the computational meshes are given the Supplementary Figure 1, and further details on the meshing process are given in (Wagner et al., 2007; Wagner et al., 2004). The TMS source was a figure-of-eight coil with two 3.5 cm radius windings made of a 25 turn, 7 mm radius copper wire, $\sigma = 5.8\times10^{7}$ S/m. The DBS source was an electrode with contacts that had a 1.5 mm height, a 1.3 mm diameter, and a 1.5 mm inter-dipole contact distance (with hollow spacing between the contacts, such that the contacts were continuous with brain tissue; as could also be modeled with two separate monopolar electrodes). The electrode contacts were made of silver, $\sigma = 6.7\times 10^{7}$ S/m, and treated as perfect conductors. The electrode lead was plastic, $\sigma = 6.7\times 10^{-15}$ S/m, $\varepsilon_r=3$. See Fig. 3, Fig. 5, and Supplementary Fig. 1 for further images of the TMS coil and DBS electrodes. The TMS coil was modeled after a Magstim figure-of-eight coil.

Field solutions were developed for three different tissue impedance sets. The first impedance set used an average of frequency independent conductivity and permittivity magnitudes, primarily reflective of ex-vivo values taken from previous brain stimulation studies, and most reflective of tissue properties used to develop neurostimulation theory ((IFAP), 2007; Foster and Schwan, 1996; Heller and Hulsteyn, 1992; Plonsey and Heppner, 1967; Wagner et al., 2004). We refer to the field solutions developed with these values as ‘tissue set 1’ or ‘frequency independent’ solutions. The second impedance set used frequency dependent impedance values reported by the IFAP ((IFAP), 2007), which is based on a parametric model of primarily ex-vivo recordings (‘tissue set 2’ or ‘frequency dependent’ solutions). The final impedance set was based on the recorded tissue permittivity and conductivity

values ('tissue set 3' or 'in-vivo recording' solutions). As less controversy surrounds fluid impedances ((IFAP), 2007; Foster and Schwan, 1996), CSF impedance values reported in the Institute of Applied Physics were used for these derived solutions. And herein we used the impedance properties of the skin to represent the entire scalp during our modeling studies, but it should be noted that the scalp is composed of not just of skin but muscle, fat, and other tissue that could significantly alter the local impedances. See Fig.2 & Sup. Table 1 for full impedance tabulation. Finally, time domain solutions were rebuilt with inverse Fourier transforms of the SSS field solutions. The transient electrical field and current density waveforms were then analyzed in terms of field magnitudes, orientations, focality, and penetration in a manner explained in prior studies by our group (Wagner et al., 2007; Wagner et al., 2004), but herein as a function of time and tissue impedance. Note, the evaluation point for TMS metrics reported in this paper (e.g. current density magnitude, electric field magnitude, etc.) is illustrated in the top right corner of Fig.3, and for DBS in Fig.5. See the supplementary methods section for further details.

2.3 Conductance Based Neural Modeling

Conductance-based compartmental models of brain stimulation were generated based on the McNeal Model (McNeal, 1976), as optimized by Rattay (Rattay, 1989), with the external driving field determined as above. Neural parameters were directly drawn from (Jones and Bawa, 1997; Traub, 1977), and the initial segment served as the focus of our calculations. We focused analysis on the 100-micron length of the axon's initial segment, divided into five 20 micron interconnected compartments, with the parameters of Table 1. Although it is known that the geometry of the nerve can effect the location and/or threshold of stimulation (Roth, 1994), to focus this study on the potential effects of tissue filtering we isolated our analysis to the region of the initial segment and assumed that the membrane voltage from stimulation at the initial segment was not affected by the properties of the soma or downstream axon. We choose the initial segment, as it contains the axon hillock, the location with the highest concentration of voltage channels, and independent of neural geometry would be the location first activated by stimulation. Studies that address the effects of neural geometry (i.e., axonal branching and/or bends, etc.) and other relevant neural components/additional channel dynamics (e.g., dendrites, soma, etc.) were left for future work.

Membrane dynamics were solved using Euler's method at a time interval of 10^{-6} sec, for details on the numerical methods see (Press et al., 2007). Neurostimulation thresholds were calculated by integrating the field solution with these compartmental models. For each stimulating waveform, source, and tissue property model, we performed an iterative search to find the smallest constrained input (TMS constrained coil currents, DBS constrained electrode currents, and DBS constrained electrode voltages) that generated an action potential, all reported in terms of peak waveform values of the constrained input. For TMS coil current inputs, we calculate the thresholds for neurons oriented approximately parallel to the figure-of-eight coil intersection (along the composite vector in Fig.3) and oriented approximately normal to the gray matter-CSF tissue-boundary. For DBS constrained current inputs, we calculate the thresholds for neurons oriented parallel to the electrode shaft. Although it was expected that the thresholds would be the same for the varied impedance

sets for the voltage constrained DBS models (as we used a variation of the McNeal model based on a voltage based activation function), they were also calculated as a redundancy check of the integrated field solver and neuromembrane methods.

2.4 Statistical Analysis

We compared the electromagnetic field properties and neural thresholds across the three tissue impedance sets for TMS and DBS stimulation sources. For each stimulation field, we compared Root Mean Square (RMS) current densities, peak current densities, RMS electric field magnitudes, peak electric field magnitudes, and the RMS displacement to ohmic current density ratios. We also compared neural thresholds computed for conductance-based neural models of the human motor neuron. For each comparison, statistical significance was determined by Wilcoxon signed-rank tests at a significance level of $p < 0.05$ (against a null hypothesis that differences in these values are due only to computational differences in the FEM equally likely to affect any of the impedance sets) (Rosner, 2010).

For more information on the methods see the supplementary materials.

3. Results

3.1 Tissue Recordings

We first measured the conductivity and permittivity values of head tissues to applied electromagnetic fields in a frequency range from 10 to 50,000 Hz in-vivo. The results of these measurements are shown in Fig.2 as a function of stimulation frequency compared to impedance sets used previously to generate neurostimulation models (and in Sup. Table 1). Recorded conductivity values were on the order of magnitude reported from past studies, but demonstrated a slightly more pronounced frequency response for gray and white matter (Fig. 2, top row). The low frequency permittivity values recorded for gray matter and white matter (~50Hz and lower), were slightly lower or similar in magnitude to those reported by Gabriel (Gabriel et al., 1996b) and reflected in the IFAP tissue set ((IFAP), 2007) (*i.e., 'tissue set 2'*). However, the largest differences between our tissue impedance recordings and those reported and used for past brain stimulation studies were seen in the tissues' relative permittivity magnitudes from the middle to the upper band of frequencies analyzed (Fig.2, bottom row). For example in Fig.2, at a 5 kHz center point of the typical TMS frequency band (Wagner et al., 2007; Wagner et al., 2004), the recorded relative permittivity magnitudes for the gray matter (solid black line) was approximately 1.5 orders of magnitude higher than those reported in primarily excised tissues of the Institute of Applied Physics Database ((IFAP), 2007) (dotted black line, 'tissue set 2') and over five orders of magnitude higher than values most commonly used in past brain stimulation studies(dashed black line, 'tissue set 1')(Wagner et al., 2004). Finally, we also found that permittivity and conductivity decreased in magnitude with time post tissue injury/death, approaching many ex-vivo values reported in the literature ((IFAP), 2007), and following tissue trends seen with post mortem changes in higher frequency bands (Schmid et al., 2003)- see Sup. Fig. 2 for these results.

3.2 Tissue effects on the TMS fields

To calculate the electromagnetic fields generated during TMS, we constructed MRI guided FEMs of the human head based on the individual tissue impedance properties recorded in-vivo (tissue set 3) and with tissue sets used in past modeling studies (tissue sets 1-2, primarily developed from ex-vivo values). We then compared the TMS induced, time dependent, field distributions, as a function of these different tissue impedance sets. Spatial and temporal snapshots of the resulting current densities for one stimulation waveform (TMS 3, triphasic wave) are shown in Fig. 3& 4. The top panel of Fig.3 shows the stimulation current input in the TMS coil on the left and the resulting current waveforms directly under the coil in the cortex for the different tissue impedance sets evaluated. The magnitude of the current density from the models based on the in-vivo recordings (red line, 'tissue set 3') is notably higher than that of either solution based on the other tissue recordings (blue and green lines, tissue sets 1 & 2), primarily as a function of higher average conductivities. The electric fields also showed altered behavior as a function of tissue impedance, but with significant decreases in the magnitude for tissue set 3 (Fig. 4, Sup. Table 2A). The center and lower panels of Fig.3 show the spatial and temporal composition of the current density in terms of ohmic and displacement currents. While the current density is primarily driven by ohmic mechanisms in all solutions, there are sizeable displacement components in the *in-vivo* recording based model solutions compared to the solutions from the other tissue sets (approximately 4X the RMS ohmic/displacement current ratio to the solution from the past frequency dependent tissue models). Differences were also seen in terms of focality of the current density distribution. For example, the maximum cortical current density areas (defined as the surface areas on the cortex where the current density was greater than 90% of its maximum value) were 174 mm^2, 163 mm^2, and 216 mm^2 for tissue sets 1-3, respectively, demonstrating a greater current spread in the in-vivo tissue recording model (Middle row Fig.3). Fig.4 shows the temporal behavior of the induced electric field and current density broken up into components tangential and normal to the gray matter surface. For all of the solutions at the evaluation site, the electric field and current density were primarily composed of vector components tangential to the coil face (approximately aligned with the composite vector, and nearly tangential to the CSF-gray matter boundary at the location of evaluation). However, the waveforms from the in-vivo recordings and past tissue measurements had distinct, directionally dependent temporal dynamics; the vector field components showed the greatest variation in the direction approximately normal to the tissue boundaries (Fig. 4, Sup.Table.2.A).

These findings were consistent across the 15 distinct stimulation waveforms tested and in each case the modeling solutions developed from our *in-vivo* recordings ('tissue set 3') were significantly different (in current density, electric field magnitude, and stimulation waveform shape/dynamics) than solutions from tissue sets 1 and 2, primarily developed with *ex-vivo* impedance recordings (See Sup.Table.2.A and Sup.Table.4).

3.3 Tissue effects on the DBS fields

We also constructed MRI guided FEMs of the human head to calculate the fields generated during DBS. Time dependent solutions of the voltage constrained DBS field distributions also demonstrated significant differences based on tissue impedance. Spatial and temporal

snapshots of the resulting current densities from one stimulation waveform (Charge balanced, 600 microsecond pulse) are shown in Fig.5. The top panel shows the voltage-constrained waveform across a dipole stimulating electrode on the left, and the resulting current waveforms at the dipole center for the different impedance sets on the right. For the different impedance sets in the inset, the magnitude of the current density in the model with in-vivo impedance set has a significantly larger initial peak and altered temporal dynamics compared to those developed with the other tissue impedance sets (tissue sets 1 & 2). The center and lower panel show the spatial and temporal composition of the current density at the dipole center in terms of ohmic and displacement components. As with the TMS fields, ohmic mechanisms are primary across all solutions, but the displacement current magnitudes represent a larger component of the in-vivo recording based modeling solutions compared to the other solutions, approx. 2.3X that of the frequency dependent impedance model solution (Fig.5, Sup.Table.2.B). Additionally, we determined the electric fields and current densities for current constrained DBS stimulation waveforms; time dependent solutions of the DBS generated field distributions demonstrated analogous differences based on the tissue impedances. The resultant electric fields were decreased in magnitude in the in-vivo tissue recording based solutions compared to the other solutions. By constraint, the total current density magnitude was the same across solutions; but, there were significant differences in the current density composition across the solutions. As in the other systems studied, the in-vivo solutions demonstrated more pronounced displacement currents in the tissues compared to the solutions from the other impedance set (Sup.Table.2.B). Both the voltage and current constrained DBS field solutions were confined to the region of gray matter in which the electrodes were placed and negligible at tissue boundaries. Thus there were no effects at the tissue boundaries in these solutions (Fig.5, Sup.Table.2.B).

As with TMS, these findings were consistent across the 15 distinct stimulation waveforms tested, resulting in significantly different current densities, electric field magnitudes, and stimulation waveform shape/dynamics in a source dependent manner when comparing the model solutions of the *in-vivo* and the other tissue impedance sets (Sup.Table.2.B, Sup.Table.4).

3.4 Tissue effects on neural response

We developed conductance-based models of neurons driven by the fields derived from the MRI guided FEMs. We compared the neurostimulation thresholds and membrane dynamics for these neurons responding to the external stimulating fields (for both TMS and DBS sources) in tissues corresponding to the three different tissue sets. The thresholds are tabulated for each stimulation waveform and condition in Fig.6 A&B, Sup. Table 3, and Sup. Figure 3. The predicted stimulation thresholds were higher for nearly all stimulation conditions in the in-vivo recording based systems compared to the other modeled tissue sets due to the increased tissue impedances and resulting attenuation of the electric fields. Across the 15 stimulation waveforms and sources tested (TMS and DBS (for current constrained inputs)), the in-vivo tissue impedance recording based stimulation thresholds were significantly higher than their other counterparts and demonstrated a significant impact of the capacitive mechanisms on initiating spiking activity at the neural membranes (see Figs. 3-6, Sup. Fig. 3, Sup.Table 3 & 4).

4. Discussion

4.1 Tissues

The recorded impedance properties of the skin, skull, gray and white matter differed substantially compared to past tissue impedance values used for characterizing the fields of neurostimulation. Conductivities were generally within the range of past reported magnitudes used for brain stimulation studies, with a slightly greater frequency response, but permittivities differed greatly in magnitude and frequency response to values typically implemented in neurostimulation modeling ((IFAP), 2007; Foster and Schwan, 1996; Gabriel et al., 1996a; Wagner et al., 2007; Wagner et al., 2004). In particular, the low frequency permittivity values that we recorded (i.e., 'tissue set 3') for gray matter and white matter (~50Hz and lower), were slightly lower or similar in magnitude than those reported by Gabriel and reflected in the IFAP tissue sets (i.e., 'tissue set 2') but approximately 1.5 orders of magnitude higher than those IFAP values at 5 kHz, the center point of the typical TMS frequency band (and substantially higher than values in 'tissue set 1' throughout the entire frequency band).

Such sizeable differences in the overall permittivity values for gray and white matter are not surprising as the majority of tissue impedance values used for neurostimulation modeling and analysis were developed from *ex-vivo* models where cell degeneration and/or death has been demonstrated to alter tissue impedance properties in higher frequency bands (Burdette et al., 1986; Schmid et al., 2003; Surowiec et al., 1986)- and as we demonstrated within the neurostimulation frequency band with infarcted tissue (Sup.Fig.2). Furthermore, as discussed by other authors, (Martinsen, 2000; Pethig and Kell, 1987), low frequency dispersion effects appear to be the first to dissipate on tissue death/degeneration (or are potentially affected more by cell/tissue degeneration than those of the higher frequency dispersions).

Other *in-vivo* impedance recordings have been made in brain tissue (Burdette et al., 1986; Kraszewski et al., 1982; Logothetis et al., 2007; Peyman et al., 2007; Schmid et al., 2003; Stuchly et al., 1981). These studies have primarily been made in frequency bands above the frequencies we analyzed, making direct value comparisons inapplicable; except for (Logothetis et al., 2007) who studied brain tissue from 10-5,000Hz. Their study concludes that brain tissue should be considered frequency independent and entirely ohmic, with reported tissue conductivity values within the range we measured. These conclusions differ from ours, and the other *in-vivo* studies of impedances over multiple frequencies (Kraszewski et al., 1982; Peyman et al., 2007; Schmid et al., 2003; Stuchly et al., 1981), which all demonstrate frequency dependent impedance responses with decreasing capacitance and increased conductance as a function of frequency, in agreement with theories of low frequency alpha dispersion in tissues (see Sup Fig.2 for further discussion). Furthermore, the range of permittivity values and/or the impedance trends that we demonstrated were generally consistent with measures from studies in which values were recorded under in-vivo conditions in other non-brain tissue types, and similar in behavior to some *in-vitro* bone measures (Akhtari et al., 2002; Behari and Singh, 1981; Gabriel et al.,

1996a; Saha and Williams, 1995; Yamamoto and Yamamoto, 1976)-see Sup. Fig. 2 for further discussion.

Overall, we demonstrated that living tissue carries currents through both dipole and ionic mechanisms, in a frequency dependent manner. Although ohmic mechanisms are primary, permittivities are of sufficient magnitude to support significant displacement currents. These results provide further evidence to long-standing tissue alpha dispersion theories (Dissado, 1990; Foster and Schwan, 1996; Pethig and Kell, 1987; Schwan, 1963).

4.2 Tissue effects on fields

There were consistent, significant alterations of the TMS and DBS field distributions in the brain when comparing the solutions from the in-vivo tissue impedance recordings with those from past ex-vivo values commonly used for modeling brain stimulation. Although tissue properties will affect every electrical-neurostimulation technique, they will maximally impact stimulation fields when transient sources are located external to the targeted tissue, because the fields will be constrained by not just the adjacent tissues, but by all of the tissues in between the stimulation source and the targeted tissue. This could impact dosing related predictions of targeting, focality, and/or waveform dynamics made in different ways depending on the specific stimulation technology used (Wagner et al., 2007). For instance, DBS demonstrates comparable field spreads with decreased electric field magnitudes between tissue sets 1 & 2 solutions (ex-vivo measures) and our in-vivo recording based solutions, but TMS demonstrates increased field spreads and decreased electric field magnitudes. Accordingly, DBS volumes of activation (VOA) could be overestimated with the ex-vivo tissue guided modeling predictions compared to the in-vivo set used (although current technologies can already predict this, for instance see (Butson and McIntyre, 2005; Grant and Lowery, 2010; Wei and Grill, 2009)). On the other hand, the TMS VOAs would be under-predicted as the electric field attenuation is less drastic compared to the tissue-boundary influenced field spread (this would not be predicted with current technologies used to predict stimulation (Wagner et al., 2007)). Furthermore, transient stimulation techniques that drive fields across multiple boundaries demonstrate increasingly complicated temporal dynamics based on the tissue-boundary conditions. For instance, when one examines the TMS field behavior for vectors approximately tangential and normal to the coil face-tissue boundaries (Fig.4), the waveforms have distinct directional dependent temporal dynamics resulting from the tissue filtering across multiple boundaries. The normal electrical fields were impacted more than the tangential electrical fields, as most likely the impact of the different tissue sets on the tangential electrical fields was minimized due to the fact that tangential electric fields are continuous across boundaries. Nonetheless, with more realistic anatomical models, the boundary conditions could become more complex. However in many DBS implementations, where the stimulatory fields are confined to a single tissue, the boundary effects will be limited to those at the electrode interface (and assessable with current DBS technology, e.g., (Butson and McIntyre, 2005)).

Thus, clinical technologies that are currently used to predict dose-related stimulation metrics are more accurate for static noninvasive technologies like transcranial direct current stimulation (Datta et al., 2009; Miranda et al., 2012) and transient invasive technologies like

DBS (Butson and McIntyre, 2005; Wei and Grill, 2009). However, technologies used for transient noninvasive methods often misrepresent dosing-metrics which could result in dosing related side-effects (Wagner et al., 2007). Note, we implemented simplified representations of tissue anatomy to highlight tissue filtering; but ultimately, clinical systems focused on transient fields will need to account for not only these effects, but also more realistic anatomies/heterogeneities (such as by Miranda and Datta (Datta et al., 2009; Miranda et al., 2012)), additional tissues, and tissue properties (such as anisotropy).

Importantly, tissue filtering will have an impact on all systems delivering stimulation waveforms with temporal dynamics related to specific neural structures. Tissues form a filtering network of capacitive and resistive elements, none of which should be ignored, as currents in the tissues are carried through both ionic and dipole mechanisms and the fields are constrained by both resistive and capacitive tissue properties.

4.3 Neural response

Predicted stimulation thresholds were consistently higher for the in-vivo systems (based on tissue set 3 models) compared to those resulting from the tissue set 1 and 2 models (primarily based on ex-vivo tissue systems). The higher thresholds for the in-vivo systems were due to the increased tissue impedance attenuation of the stimulatory electric fields (Fig. 3-6, Sup.Table.2&3). In comparison to published experimental neural data, all of the predicted thresholds (for tissue sets 1-3) were within published experimental ranges, but the in-vivo recording based field waveforms (tissue set 3 solutions) demonstrated the greatest similarity in behavior to direct waveform measurements with similar driving sources (Miocinovic et al., 2009; Tay, 1992; Tay, 1989)(Figs. 3-6, Sup.Table.2&3). While direct extrapolation of macroscopic results to the microscopic neural level is difficult (Agin, 1967), the findings herein present guidance for incorporating frequency dependent macroscopic tissue filtering effects with conductance based neural models to predict frequency dependent neural responses to external stimulation (Dissado, 1987). Such studies could be used to design more efficient stimulation technology or to better interpret the cellular impact of stimulation studies.

4.4 Future studies

We provide evidence of tissue alpha dispersion behavior in the frequency band of stimulation (i.e., increasing permittivity and decreasing conductance as a function of decreasing frequency), which was first demonstrated in muscle in the early 50’s (Schwan, 1954, 1963) and subsequently in brain and other head tissues (e.g., see reviews such as (Foster and Schwan, 1989; Gabriel et al., 1996a)). Our results demonstrated the presence of tissue impedance filtering properties significant enough to impact both stimulation fields and stimulation responses. However, future works, such as large-scale studies across multiple species, are needed to further bear out these results and to explore issues not addressed in this initial study (e.g., effects of tissue pathologies in the human brain).

An important caveat needs to be made with regards to current, past, and future impedance measurements. It is known that electrode polarization can lead to uncertainties in tissue impedance measurements (Schwan, 1963). While in our study we controlled for this

phenomenon by directly implementing the approach of Gabriel (Gabriel et al., 1996b), and also using well characterized materials for our probe interface (i.e., platinum) and a high resolution recording system (Schwan, 1963; Schwan, 1966, 1992), a properly applied 4-point method, including a null balance procedure and recording resolution capable of resolving capacitance, could further improve our recordings (Schwan, 1963; Schwan and Ferris, 1968). This is important, since as demonstrated by Schwan (Schwan, 1963; Schwan and Ferris, 1968) while describing the correct use of the 4-point method, an improper implementation of this approach can lead to measures which do not adequately resolve the frequency dependent tissue response, and potentially lead to the incorrect conclusion that tissue-current interactions are entirely ohmic. However, improved recording techniques will allow for improved resolution, the ability to investigate further tissues, and the possibility of less invasive recordings (Singh et al., 1979).

The outcomes of future explorations could be used to evaluate neurostimulation safety and dosing considerations. For example, stimulation induced tissue injury has classically been explored in terms of a stimulating waveforms' total current density amplitude, charge per phase, and total charge (McCreery and Agnew, 1990). However, an exploration of dipole and free charge effects (i.e., displacement and ohmic currents) offers a method to further characterize processes such as electrochemical reactions, heating, and electroporation, which can be linked to tissue injury (McCreery and Agnew, 1990; McCreery et al., 1988). Furthermore, additional studies need to be completed in assessing the effects of pathologies on tissue electromagnetic properties (e.g., tumor, stroke). For instance, (Singh et al., 1979) demonstrated elevated permittivities in malignant tissue, and iron deposits in tissues following stroke could impact local tissue conductivity (Novak et al., 2001)- both of which could impact simulation fields.

Although future studies are mandated, electromagnetic field based safety and dosing criteria should not be directly matched across different neurostimulation (and/or imaging) techniques unless controlled for altered tissue effects and/or different spectral source characteristics. For example, TMS stimulation is often deemed safe for patients if they meet MRI inclusion criteria. However, the slew rates and frequency range in which MRI and TMS techniques operate are different and the expected tissue responses between the two are not readily comparable. Irrespective of spatial differences in the source fields and the exact tissue impedances under study, a more valid safety comparison between the two techniques would require matching the methodologies' source power spectrums as a function of total energy and power provided. Conversely, one could explore matching spectral field characteristics across different methodologies to optimize stimulation parameters for efficacy, or optimize the different stimulation waveforms based on the spectral characteristics for device efficacy (e.g., tuned TMS waveforms for specific neural responses) or device efficiency (e.g., optimize DBS waveforms for battery life). These all remain areas of active research, and future studies in these areas need to be completed before the full implementation of such ideas can be put into current practice.

4.5. Conclusions

In sum, we here demonstrated the effects of frequency dependent tissue impedances on the stimulation fields of TMS and DBS with tissue properties derived from the literature and from in-vivo tissue recordings. Future large-scale tissue studies, across multiple species and pathological states, should ultimately be pursued to gain further knowledge of the effects of electromagnetic tissue interactions on neurostimulation. Fundamentally, much like chemistry guides the development of pharmaceuticals, biophysics based studies can guide the development of neurostimulation methodologies and dosing standards.

Supplementary Material

Refer to Web version on PubMed Central for supplementary material.

Acknowledgments

Support Statement: This material is based in part upon work supported by the Defense Advanced Research Projects Agency (DARPA) under Contract No. W31P4Q-09-C-0117. This work is also supported in part by Award Number R43NS062530 and 1R44NS080632 from the National Institute of Neurological Disorders And Stroke. The content is solely the responsibility of the authors and does not necessarily represent the official views of the National Institute of Neurological Disorders And Stroke, the National Institutes of Health, or DARPA.

References

Gabriel, C. (IFAP), I.F.A.P. Compilation of the dielectric properties of body tissues at RF and microwave frequencies. Dielectric Properties of body tissues in the frequency range of 10 Hz to 100 GHz- Work reported from the Brooks Air Force Base Report. 2007. http://niremf.ifac.cnr.it/tissprop/

Agin D. Electroneutrality and electrodiffusion in the squid axon. Proc Natl Acad Sci U S A. 1967; 57:1232–1238. [PubMed: 5231728]

Akhtari M, Bryant HC, Mamelak AN, Flynn ER, Heller L, Shih JJ, Mandelkern M, Matlachov A, Ranken DM, Best ED, DiMauro MA, Lee RR, Sutherling WW. Conductivities of three-layer live human skull. Brain topography. 2002; 14:151–167. [PubMed: 12002346]

Bedard C, Kroger H, Destexhe A. Modeling extracellular field potentials and the frequency-filtering properties of extracellular space. Biophys J. 2004; 86:1829–1842. [PubMed: 14990509]

Behari J, Singh S. Bioelectric characteristics of unstressed in vivo bone. Med Biol Eng Comput. 1981; 19:49–54. [PubMed: 7278407]

Bossetti CA, Birdno MJ, Grill WM. Analysis of the quasi-static approximation for calculating potentials generated by neural stimulation. J Neural Eng. 2008; 5:44–53. [PubMed: 18310810]

Burdette EC, Friederich PG, Seaman RL, Larsen LE. In Situ Permittivity of Canine Brain: Regional Variations and Postmortem Changes. IEEE Trans on Microwave Theory and Techniques MTT. 1986; 34:38–50.

Butson CR, McIntyre CC. Tissue and electrode capacitance reduce neural activation volumes during deep brain stimulation. Clin Neurophysiol. 2005; 116:2490–2500. [PubMed: 16125463]

Datta A, Bansal V, Diaz J, Patel J, Reato D, Bikson M. Gyri-precise head model of transcranial direct current stimulation: improved spatial focality using a ring electrode versus conventional rectangular pad. Brain Stimul. 2009; 2:201–207. 207 e201. [PubMed: 20648973]

De Geeter N, Crevecoeur G, Dupre L, Van Hecke W, Leemans A. A DTI-based model for TMS using the independent impedance method with frequency-dependent tissue parameters. Phys Med Biol. 2012; 57:2169–2188. [PubMed: 22452983]

Dissado LA. Ion transport through nerves and tissues. Comments Mol Cell Biophys. 1987; 4:143–169.

Dissado LA. A fractal interpertation of the dielectric response of animal tissues. Phys Med Biol. 1990; 35:1487–1503. [PubMed: 2287626]

Foster KR, Schwan HP. Dielectric properties of tissues and biological materials: a critical review. Critical reviews in biomedical engineering. 1989; 17:25–104. [PubMed: 2651001]

Foster, KR.; Schwan, HP. Dielectric Properties of Tissues. In: Polk, C.; Postow, E., editors. Biological Effects of Electromagnetic Fields. CRC Press; New York: 1996. p. 25-102.

Gabriel C, Gabriel S, Corthout E. The dielectric properties of biological tissues: I. Literature survey. Phys Med Biol. 1996a; 41:2231–2249. [PubMed: 8938024]

Gabriel S, Lau RW, Gabriel C. The dielectric properties of biological tissues: II. Measurements in the frequency range 10 Hz to 20 GHz. Phys Med Biol. 1996b; 41:2251–2269. [PubMed: 8938025]

Grant PF, Lowery MM. Effect of dispersive conductivity and permittivity in volume conductor models of deep brain stimulation. IEEE Trans Biomed Eng. 2010; 57:2386–2393. [PubMed: 20595081]

Heller L, Hulsteyn DBv. Brain stimulation using electromagnetic sources: theoretical aspects. Biophysical Journal. 1992; 63:129–138. [PubMed: 1420862]

Jones KE, Bawa P. Computer simulation of the responses of human motoneurons to composite 1A EPSPS: effects of background firing rate. J Neurophysiol. 1997; 77:405–420. [PubMed: 9120581]

Kraszewski A, Stuchly MA, Stuchly SS, Smith AM. In vivo and in vitro dielectric properties of animal tissues at radio frequencies. Bioelectromagnetics. 1982; 3:421–432. [PubMed: 7181965]

Kuncel AM, Grill WM. Selection of stimulus parameters for deep brain stimulation. Clin Neurophysiol. 2004; 115:2431–2441. [PubMed: 15465430]

Logothetis NK, Kayser C, Oeltermann A. In vivo measurement of cortical impedance spectrum in monkeys: implications for signal propagation. Neuron. 2007; 55:809–823. [PubMed: 17785187]

Martinsen, ØG.; G, S. Bioimpedance and Bioelectricity Basics. Academic Press; 2000.

McCreery, D.; Agnew, W. Neuronal and axonal injury during functional electrical stimulation; a review of the possible mechanisms. Annual International Conference of the IEEE Engineering in Medicine and Biology Society; IEEE; 1990. p. 1489

McCreery DB, Agnew WF, Yuen TG, Bullara LA. Comparison of neural damage induced by electrical stimulation with faradaic and capacitor electrodes. Ann Biomed Eng. 1988; 16:463–481. [PubMed: 3189974]

McNeal DR. Analysis of a model for excitation of myelinated nerve. IEEE Trans Biomed Eng. 1976; 23:329–337. [PubMed: 1278925]

Miocinovic S, Lempka SF, Russo GS, Maks CB, Butson CR, Sakaie KE, Vitek JL, McIntyre CC. Experimental and theoretical characterization of the voltage distribution generated by deep brain stimulation. Exp Neurol. 2009; 216:166–176. [PubMed: 19118551]

Miranda PC, Mekonnen A, Salvador R, Ruffini G. The electric field in the cortex during transcranial current stimulation. Neuroimage. 2012

Novak V, Kangarlu A, Abduljalil A, Novak P, Slivka A, Chakeres D, Robitaille PM. Ultra high field MRI at 8 Tesla of subacute hemorrhagic stroke. J Comput Assist Tomogr. 2001; 25:431–435. [PubMed: 11351195]

Pethig R, Kell DB. The passive electrical propeties of biological systems: their signicance in physiology, biophysics, and biotechnology. Phys Med Biol. 1987; 32:933–970. [PubMed: 3306721]

Peyman A, Holden SJ, Watts S, Perrott R, Gabriel C. Dielectric properties of porcine cerebrospinal tissues at microwave frequencies: in vivo, in vitro and systematic variation with age. Phys Med Biol. 2007; 52:2229–2245. [PubMed: 17404466]

Plonsey R, Heppner DB. Considerations of quasi-stationarity in electrophysiological systems. Bull Math Biophys. 1967; 29:657–664. [PubMed: 5582145]

Press, W.; Teukolsky, S.; Vetterling, W.; Flannery, B. The Art of Scientific Computing. 3. Cambridge University Press; 2007. Numerical Recipes.

Rattay F. Analysis of models for extracellular fiber stimulation. IEEE Transactions on Biomedical Engineering. 1989; 36:974–977.

Rosner B. Fundamentals of Biostatistics. Cengage Learning. 2010

Roth BJ. Mechanisms for electrical stimulation of excitable tissue. Critical reviews in biomedical engineering. 1994; 22:253–305. [PubMed: 8598130]

Rushmore RJ, Valero-Cabre A, Lomber SG, Hilgetag CC, Payne BR. Functional circuitry underlying visual neglect. Brain. 2006; 129:1803–1821. [PubMed: 16731540]

Saha S, Williams PA. Comparison of the electrical and dielectric behavior of wet human cortical and cancellous bone tissue from the distal tibia. J Orthop Res. 1995; 13:524–532. [PubMed: 7674068]

Schmid G, Neubauer G, Illievich UM, Alesch F. Dielectric properties of porcine brain tissue in the transition from life to death at frequencies from 800 to 1900 MHz. Bioelectromagnetics. 2003; 24:413–422. [PubMed: 12929160]

Schwan HP. Die elektrischen eigenschaften von muskelgewebe bei niederfrequenz. Z Naturforschung. 1954; 9b:245–251.

Schwan, HP. Physical Techniques in Biological Research. Academic Press; New York: 1963. Determination of Biological Impedances; p. 323-408.

Schwan HP. Alternating Current Electrode Polarization*. Biophysik. 1966; 3:181–201. [PubMed: 5982795]

Schwan HP. Electrode polarization impedance and measurements in biological materials. Ann N Y Acad Sci. 1968; 148:191–209. [PubMed: 5237641]

Schwan HP. Linear and nonlinear electrode polarization and biological materials. Ann Biomed Eng. 1992; 20:269–288. [PubMed: 1443824]

Schwan HP, Ferris CD. Four-Electrode Null Techniques for Impedance Measurement with High Resolution. Review of Scientific Instruments. 1968:481–485.

Singh B, Smith CW, Hughes R. In vivo dielectric spectrometer. Med Biol Eng Comput. 1979; 17:45–60. [PubMed: 312384]

Stuchly MA, Athey TW, Stuchly SS, Samaras GM, Taylor G. Dielectric properties of animal tissues in vivo at frequencies 10 MHz--1 GHz. Bioelectromagnetics. 1981; 2:93–103. [PubMed: 7295367]

Surowiec A, Stuchly SS, Swarup A. Postmortem changes of the dielectric properties of bovine brain tissues at low radiofrequencies. Bioelectromagnetics. 1986; 7:31–43. [PubMed: 3730000]

Tay, G. Measurement of current density distribution induced in vivo during magnetic stimulation. Marquette University; Milwaukee: 1992. p. 211

Tay, GC.; M; Battocletti, J.; Sances, A., Jr; Swiontek, T.; Kurakami, C. Measurement of magnetically induced current density in saline and in vivo. Engineering in Medicine and Biology Society, 1989. Images of the Twenty-First Century., Proceedings of the Annual International Conference of the IEEE; 1989. p. 1167-1168.

Tehovnik EJ. Electrical stimulation of neural tissue to evoke behavioral responses. J Neurosci Methods. 1996; 65:1–17. [PubMed: 8815302]

Tracey B, Williams M. Computationally efficient bioelectric field modeling and effects of frequency-dependent tissue capacitance. J Neural Eng. 2011; 8:036017. [PubMed: 21540485]

Traub RD. Motorneurons of different geometry and the size principle. Biol Cybern. 1977; 25:163–176. [PubMed: 836920]

Wagner T, Valero-Cabre A, Pascual-Leone A. Noninvasive Human Brain Stimulation. Annu Rev Biomed Eng. 2007

Wagner TA, Zahn M, Grodzinsky AJ, Pascual-Leone A. Three-dimensional head model simulation of transcranial magnetic stimulation. IEEE Trans Biomed Eng. 2004; 51:1586–1598. [PubMed: 15376507]

Wei XF, Grill WM. Impedance characteristics of deep brain stimulation electrodes in vitro and in vivo. J Neural Eng. 2009; 6:046008. [PubMed: 19587394]

Yamamoto T, Yamamoto Y. Electrical properties of the epidermal stratum corneum. Med Biol Eng. 1976; 14:151–158. [PubMed: 940370]

Abbreviations

CSF	Cerebral Spinal Fluid
DBS	Deep Brain Stimulation

FEM	Finite Element Model
HP	Hewlett Packard
IACUC	Institutional Animal Care and Use Committee
MRI	Magnetic Resonance Imaging
RMS	Root Mean Squared
TMS	Transcranial Magnetic Stimulation
VOA	Volumes of Activation

Highlights

- TMS & DBS models were generated from *in-vivo* brain tissue impedance recordings.
- The stimulation current has frequency dependent resistive and capacitive components.
- The mechanisms significantly affect modeled TMS & DBS fields and neural responses.

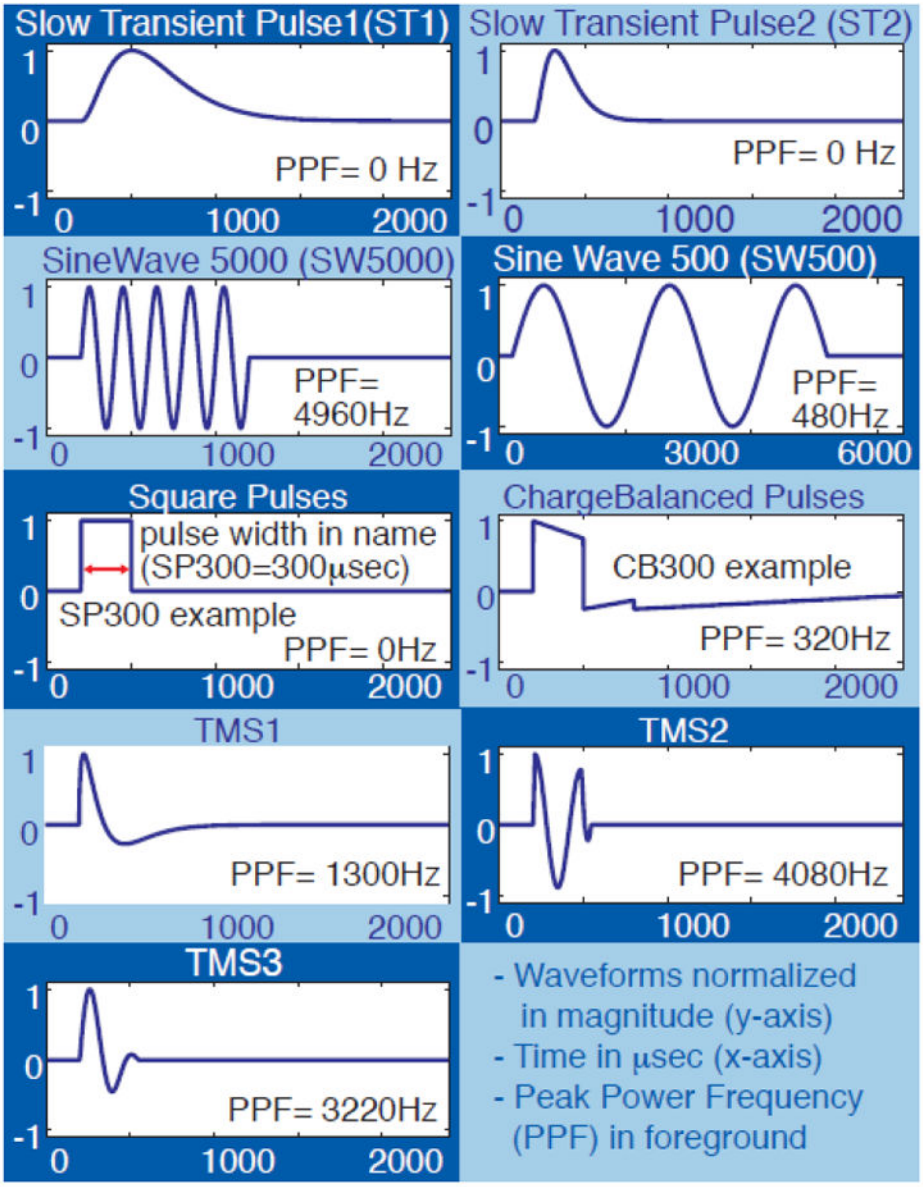

Figure 1.

Source Waveforms for the TMS coil current, DBS constrained voltage, and DBS constrained current, herein normalized to the maximum peak values. Additional square pulses (SP) and charge-balanced pulses (CB) were examined with 600, 1000, and 2000 μs pulse widths (SP's demonstrated 0 Hz peak power frequency components and the CB's 180, 100, and 40 Hz respectively). Note we evaluated each waveform across all sources (i.e., implementing typical TMS waveforms across DBS sources, and vice versa).

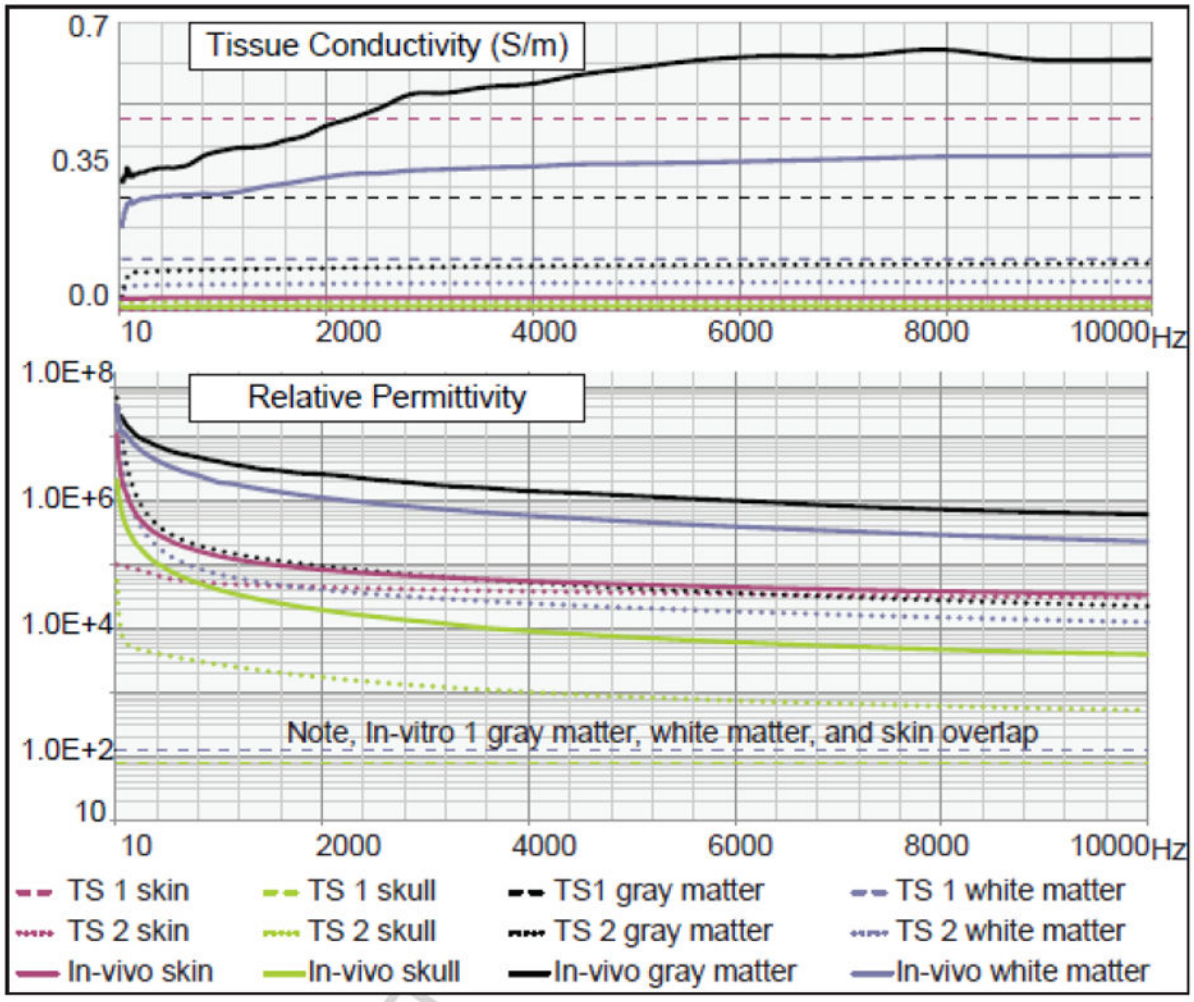

Figure 2.

Recorded Tissue Impedance Values within the Brain Stimulation Spectrum from 10 to 10,000 Hz (with comparison to values from the literature used for past brain stimulation models, primarily based on ex-vivo values). Note, tissue set 1 (TS 1) and tissue set 2 (TS 2) sets were derived from literature averages used for past brain stimulation studies (Wagner et al., 2007; Wagner et al., 2004) and from the Institute of Applied Physics database ((IFAP), 2007) respectively; these are primarily ex-vivo values that have generally served as the basis for developing neurostimulation theory (see Methods section for further details). The in-vivo values are those we recorded (tissue set 3). See Supplementary Table 1 for 10-50 KHz values.

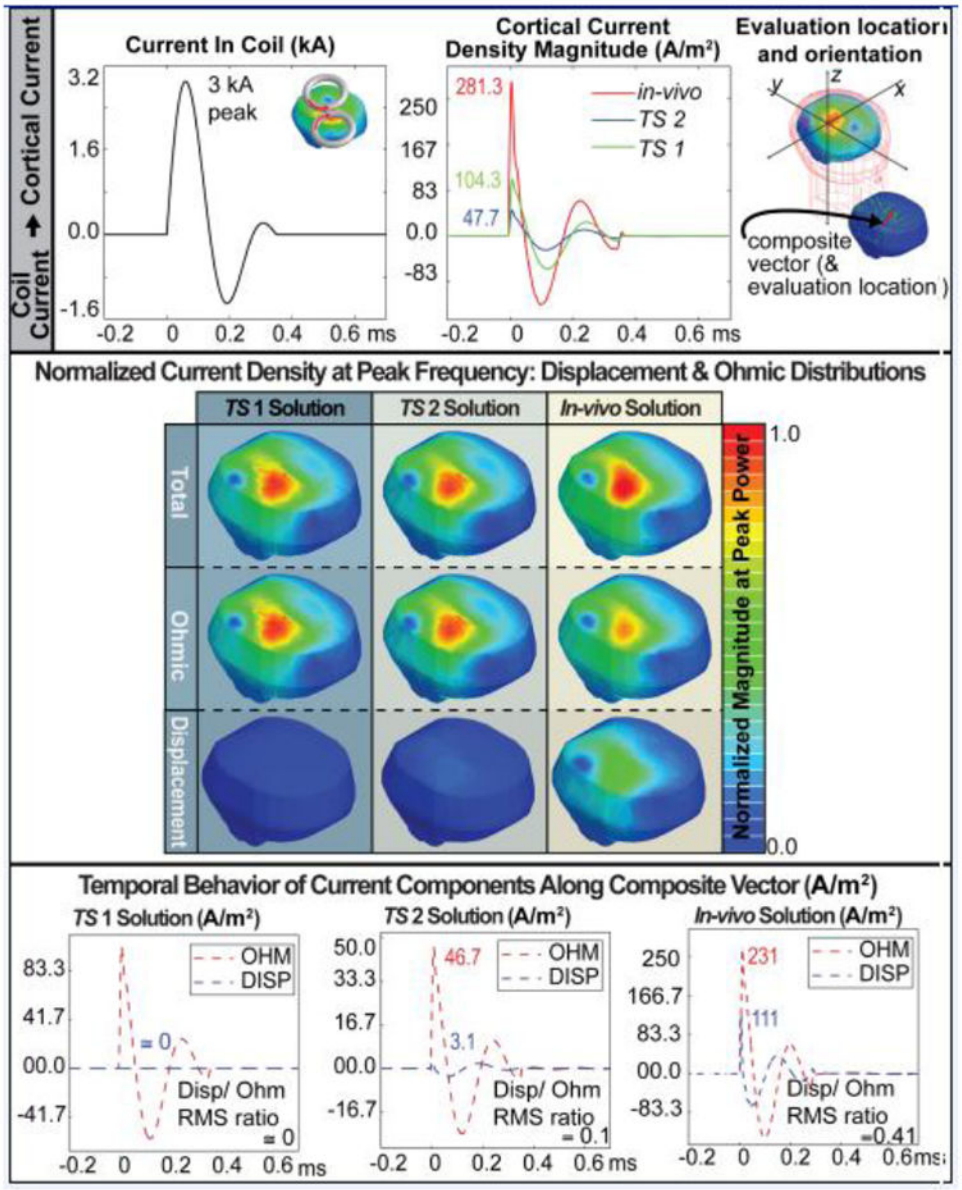

Figure 3. TMS Electromagnetic fields for the TMS 3 pulse (tri-phasic pulse)

The results are depicted for ‘tissue set 1’ (TS 1), ‘tissue set 2’ (TS 2), and our in-vivo recordings (‘tissue set 3’). The figure demonstrates the coil current, cortical current density waveforms, the composition of the cortical current densities on cortical surface at peak frequency, and the current composition as a function of time at the evaluation point (Note the evaluation point centered 2.3 cm from the coil face, this is the evaluation location for the TMS analysis unless otherwise noted. Also note root mean square (RMS) values were calculated across the pulse waveforms, (defined as the square root of the average of the squares of the original values)). The term “composite vector” corresponds to the total vector solution for the field, the “normal vector” corresponds to solution in the direction directly normal to the tissue surface at the evaluation point, and the “tangential vector” points in the

direction tangential to the tissue surface (in the direction where the individual circular coils of the figure-of-eight coils meet); this is expanded graphically in Fig.4.

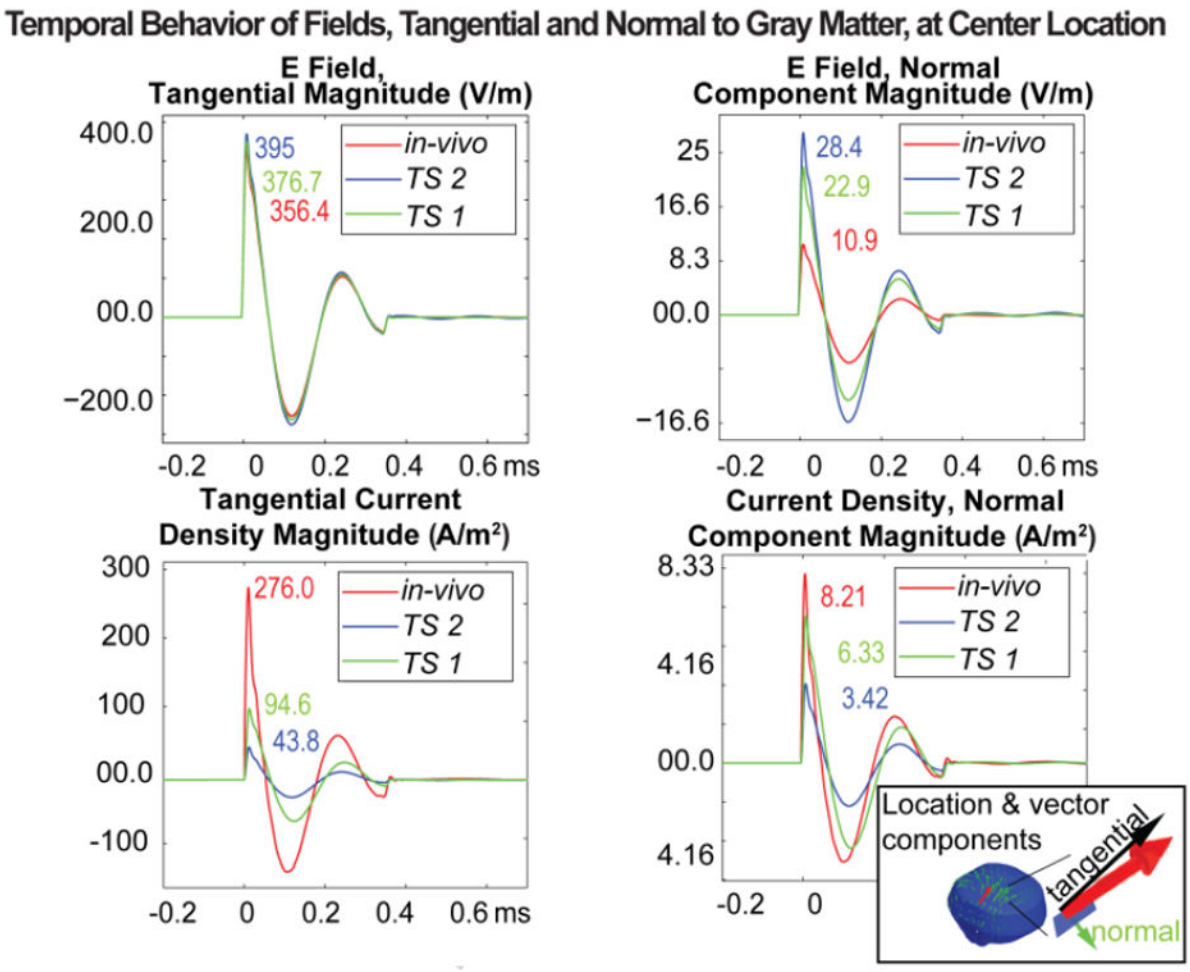

Figure 4.

TMS Electric Field and Current Densities for the TMS 3 pulse evaluated along vectors approximately tangential and normal to the cortical surface (TS 1(‘tissue set 1), TS 2 (‘tissue set 2), and in-vivo (‘tissue set 3’)).

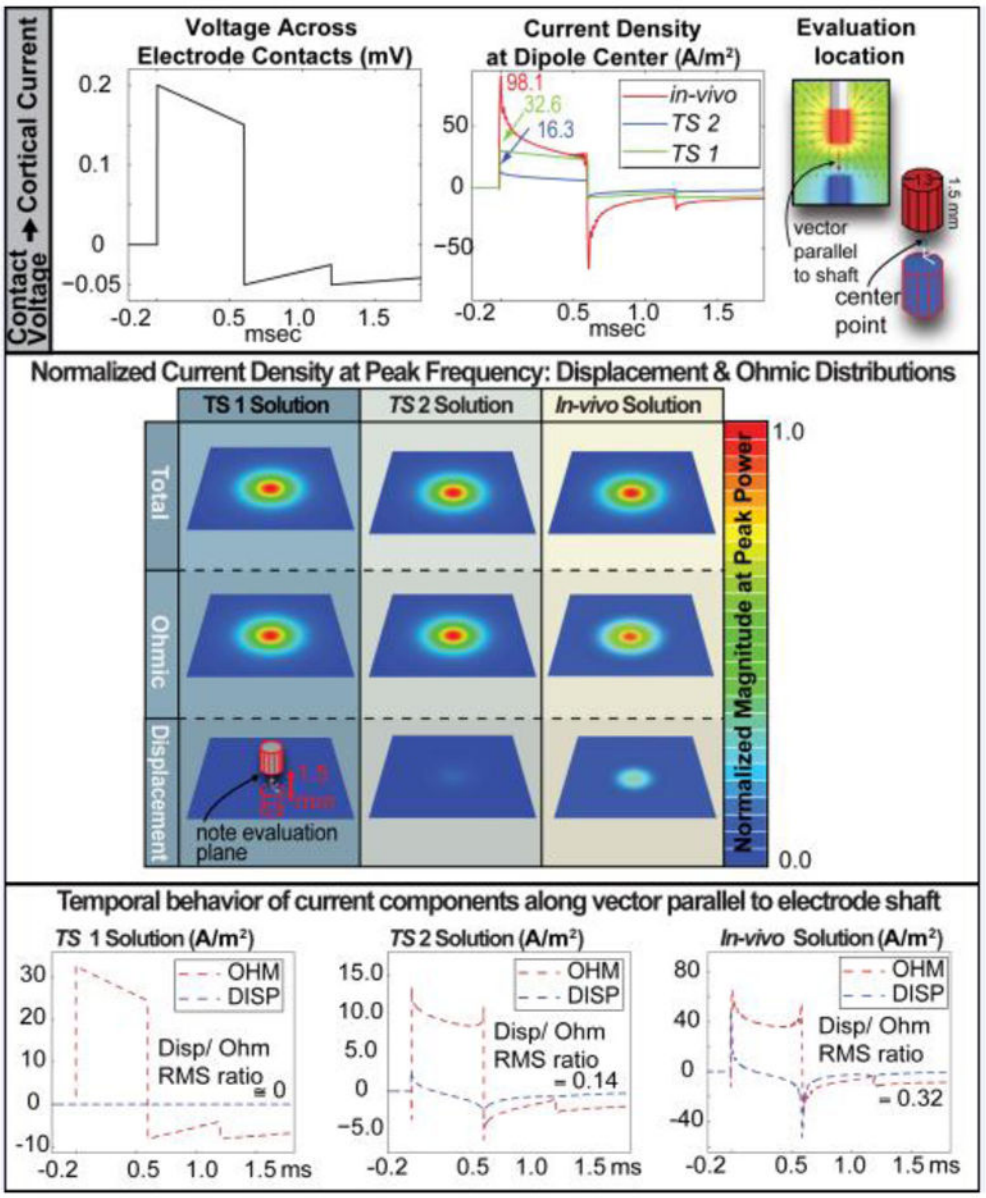

Figure 5. DBS Electromagnetic field example for the 600 μs charge balanced waveform (CB600)

Note TS 1 is 'tissue set 1, TS 2 is 'tissue set 2, and the in-vivo solutions are for 'tissue set 3'. The electrode was modeled with the DBS electrode contacts placed in the area corresponding to the location of basal ganglia. However, the resulting stimulation field was confined to within the tissue surrounding the electrode- and thus, a similar solution would result in any location where the tissue is sufficiently large to surround the electrode contacts.

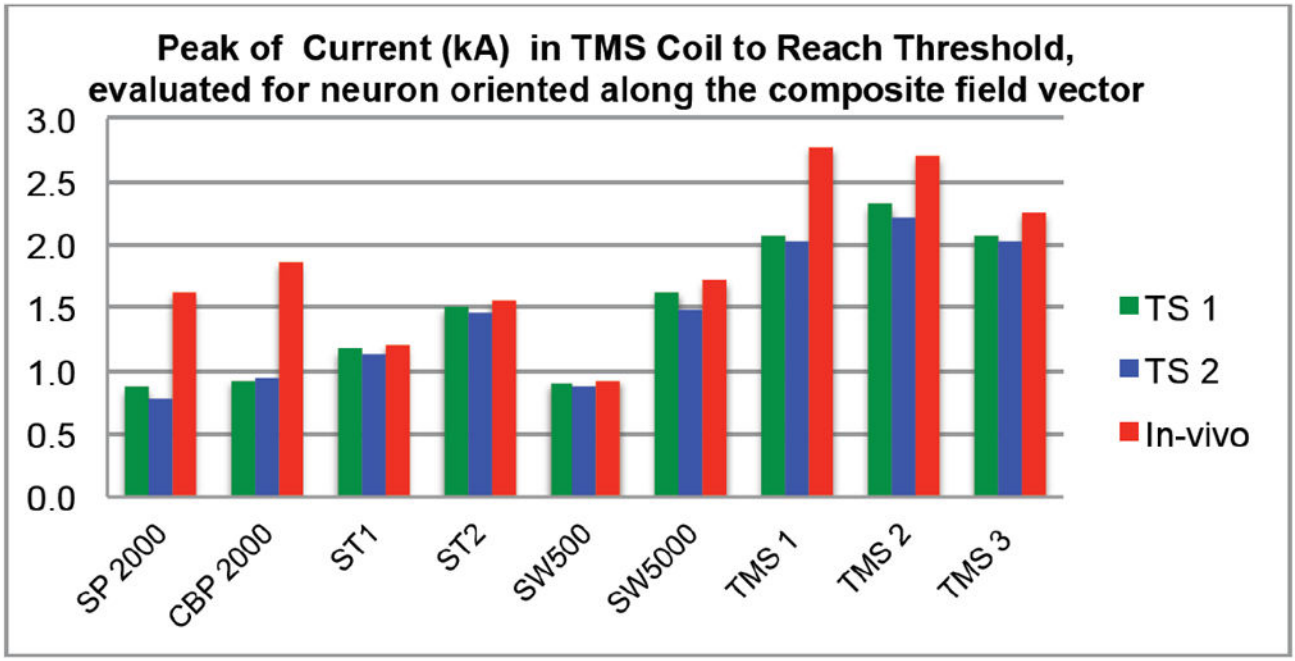

A

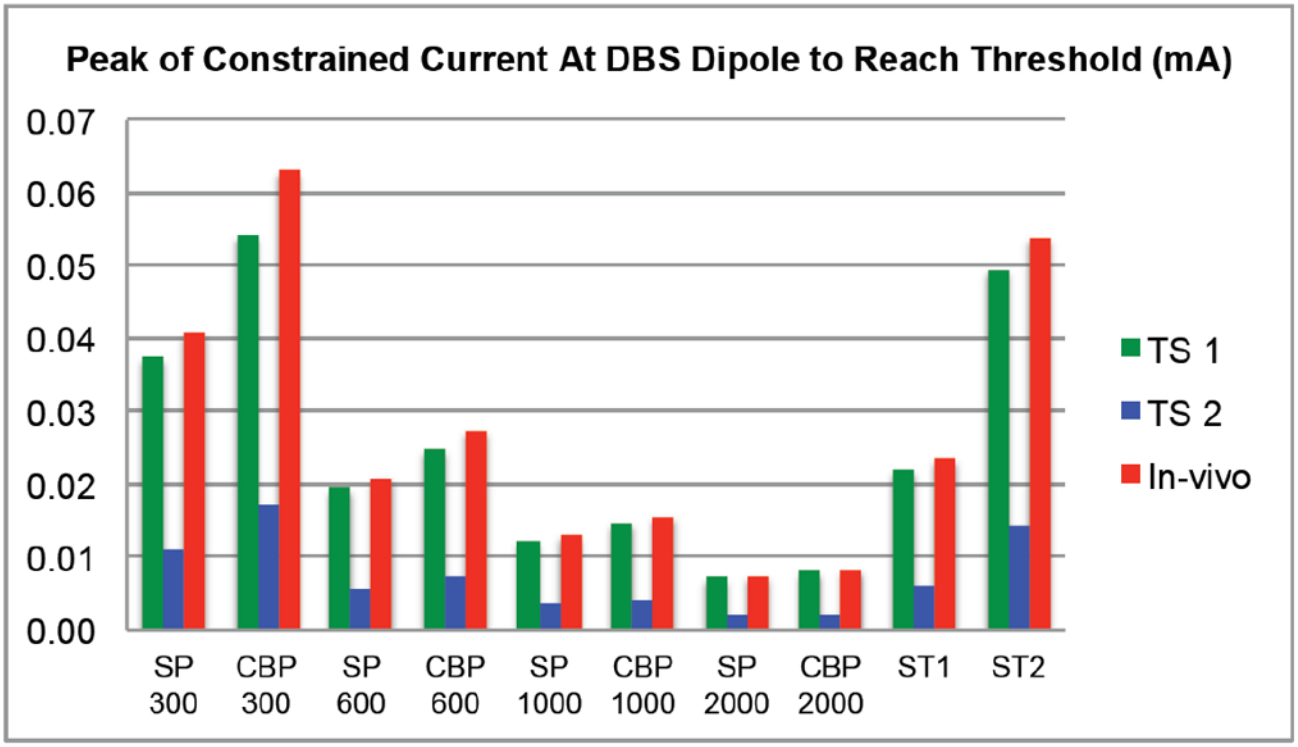

B

Figure 6.

A.TMS & B.DBS. Human Motor Neuron Thresholds as a function of the tissue properties examined for the sources and waveforms tested. TMS thresholds are evaluated at a location centered to figure-of-eight coil intersection 2.3 cm from coil face with a 25-turn air core copper coil, and the DBS thresholds at point 0.75 mm from the electrode contacts (see Figure 3 & 5 for evaluation locations). *Note* TS 1 is ‘tissue set 1, TS 2 is ‘tissue set 2, and the in-vivo solutions are for tissue set 3. See Supplementary Figure 3 and Supplementary Table 3 for further examples (herein we focus on the waveforms most relevant for each technique, as commonly used in the clinic/laboratory).

Table 1

Human Motor Neuron Membrane Properties: Initial segment properties and equations- for further details see (Jones and Bawa, 1997; Traub, 1977).

Initial segment length	100 micron
Initial segment compartment length	20 micron
Initial segment diameter	5 micron
Capacitance of membrane	1 microFarad/cm^2
Axonal resistivity	70 ohm cm
g_{Na}	500 mS/cm^2
E_{Na}	115 mV
g_K	100 mS/cm^2
E_K	-10 mV
I_{Na}	$g_{Na}*m^3*h*(V_m-E_{Na})$
I_K	$g_K*n^4*(V_m-E_{Na})$
α_m	$(4-0.4* V_m)/(e^{((1* Vm -10)/-5)}-1)$
α_h	$0.16/e^{((Vm -37.78)/-18.14)}$
α_n	$(0.2-0.02*V_m)/(e^{((Vm -10)/-10)}-1)$
β_m	$(0.4* V_m-14)/((e^{(1*Vm-35)/5})-1)$
β_h	$4/(e^{(3-0.1*Vm)}+1)$
β_n	$0.15/(e^{((Vm-33.79)/71.86)}-0.01)$